ACS APPLIED MATERIALS & INTERFACES

Research Article

www.acsami.org

Enhanced Raman Spectroscopy of Molecules Adsorbed on Carbon-Doped TiO_2 Obtained from Titanium Carbide: A Visible-Light-Assisted Renewable Substrate

Vankayala Kiran and Srinivasan Sampath*

Department of Inorganic and Physical Chemistry, Indian Institute of Science, Bangalore 560012, India

Supporting Information

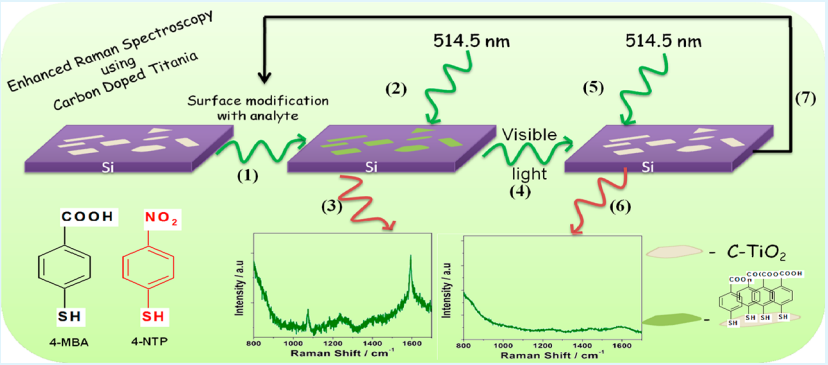

ABSTRACT: Titanium carbide (TiC) is an electrically conducting material with favorable electrochemical properties. In the present studies, carbon-doped TiO_2 (C-TiO_2) has been synthesized from TiC particles, as well as TiC films coated on stainless steel substrate via thermal annealing under various conditions. Several C-TiO_2 substrates are synthesized by varying experimental conditions and characterized by UV−visible spectroscopy, photoluminescence, X-ray diffraction, and X-ray photoelectron spectroscopic techniques. C-TiO_2 in the dry state (in powder form as well as in film form) is subsequently used as a substrate for enhancing Raman signals corresponding to 4-mercaptobenzoic acid and 4-nitrothiophenol by utilizing chemical enhancement based on charge-transfer interactions. Carbon, a nonmetal dopant in TiO_2, improves the intensities of Raman signals, compared to undoped TiO_2. Significant dependence of Raman intensity on carbon doping is observed. Ameliorated performance obtained using C-TiO_2 is attributed to the presence of surface defects that originate due to carbon as a dopant, which, in turn, triggers charge transfer between TiO_2 and analyte. The C-TiO_2 substrates are subsequently regenerated for repetitive use by illuminating an analyte-adsorbed substrate with visible light for a period of 5 h.

KEYWORDS: *titanium carbide, carbon doped TiO_2, renewable Raman substrate, visible light*

INTRODUCTION

Semiconducting oxide materials, especially titanium dioxide (TiO_2), have gained tremendous importance, because of their fascinating chemical and physical properties. TiO_2 has been used in several research areas such as biomedical devices,[1−3] energy systems,[4,5] and environmental remediation.[6−8] Research on TiO_2 gained prominence after the discovery of photosplitting of water by Fujishima and Honda.[9] The material has been recently receiving attention in the context of photovoltaic devices and other multifunctional applications.[1−8] Effective use of TiO_2 depends on the separation of photogenerated electrons and holes without recombination. Rajh et al.[10,11] have reported strategies where recombination can be suppressed via surface functionalization. It has also been reported that doping of TiO_2 with metals or nonmetals inhibits the rate of recombination of charge carriers by creating/modifying the band gap with the introduction of several sub-band-gap energy levels.[12,13]

Multifunctionality of TiO_2 has recently taken a different direction in exploring its ability to act as good Raman scattering substrates. Use of TiO_2 as substrates for Raman spectroscopy in recognition of sulfur-containing molecules[14,15] and for biodetection of analytes such as dopamine and DOPAC[16,17] has been reported. In this context, it should be mentioned that various semiconducting materials, such as ZrO_2,[17] CuO,[18] ZnO,[19] Fe_2O_3,[17] CeO_2,[17] CdS,[20] ZnS,[21] GaP,[22] PbS,[23] CdTe,[24] InAs/GaAs[25] etc., have also been reported as substrates for the detection of different analytes. Chemical-enhancement-based mechanisms have been proposed for the observed enhancement in Raman signals.[14−25]

In the case of metallic substrates, surface-enhanced Raman scattering (SERS) is mainly due to electromagnetic (EM) contribution that provides improved Raman cross section to the analyte resulting in an enhancement of signal. Also, it has

Received: February 27, 2012
Accepted: June 27, 2012
Published: June 27, 2012

dx.doi.org/10.1021/am300349k | ACS Appl. Mater. Interfaces 2012, 4, 3818−3828

been generally accepted that the EM mechanism does not require adsorptive interactions of analytes with a surface but it should be confined in the vicinity of local electric field around the surface.[17] Unlike metallic substrates, enhancement in Raman spectral signals observed in the case of semiconductors is mainly attributed to chemical effects (CM), where adsorptive interactions of analyte with the substrate play a crucial role. This leads to the formation of charge-transfer complexes that absorb light at the extinction frequency, yielding resonance Raman scattering.[26−28] In contrast to metals, most of the semiconductors possess surface plasmon peaks in the infrared region.[14] Hence, the origin of enhancement in the case of semiconductors is primarily CM-type, as reported by several research groups.[14−25] Indeed, it is advantageous to study Raman scattering on non-noble-metal substrates like semiconductors, since properties that are associated with semiconductors, such as band gap, phonon coupling strength, exciton Bohr radius, and surface morphology, are tunable.[29] The importance of SERS as a promising analytical tool can be improved only by developing inexpensive, stable, and reproducible substrates that can be easily prepared. There are few reports on renewable SERS substrates based on Au/TiO_2,[30−32] Au/ZnO,[33] and Ag/BN nanosheets,[34] where the surface is reproduced by means of stimuli like UV light,[30−33] high-temperature air oxidation,[34] etc.

The present study is directed at the preparation and characterization of carbon-doped TiO_2 (C-TiO_2), compared to undoped TiO_2, as an active substrate to achieve enhancement of Raman signals. The activity toward 4-mercaptobenzoic acid (4-MBA) and 4-nitrothiophenol (4-NTP) has been followed using C-TiO_2 prepared under different conditions. It is observed that the enhancement of Raman signal can be tuned by varying the amount of carbon dopant in TiO_2. Carbon is a nonmetal dopant. The photostability of nonmetal doped TiO_2 is likely to be better than that of transition-metal-doped TiO_2, because of the latter's poor photostability.[12] This is indeed the case as shown below, where a C-TiO_2 substrate is regenerated by visible-light illumination, which is a green approach to produce renewable substrates for periodic use. One advantage of the present protocol is also in the use of visible radiation, which will lead to renewability under sunlight; this is an economically viable and green methodology. We have avoided the use of the term "SERS" to describe enhancement of Raman signals using C-TiO_2, since the enhancement is not EM-based, although there is published literature wherein semiconductor substrates giving rise to CM-based enhancement are called SERS substrates.[14−25]

EXPERIMENTAL SECTION

Materials: Preparation. TiC powder was obtained from MaTeK, Germany. 4-MBA and 4-NTP were products of Aldrich, USA. All solutions were prepared using pure ethanol (HPLC grade) solvent obtained from Polysales, India. TiC films coated on stainless steel (SS) was prepared via cathodic arc deposition technique as reported elsewhere (see the Supporting Information).

Various C-TiO_2 substrates were prepared from TiC powders and TiC films by oxidative treatment under ambient conditions. Briefly, a certain amount of TiC powder/film on a stainless steel (SS) substrate was subjected to thermal treatment at different temperatures for a certain period of time (for experimental conditions, see Table 1). The initial black color of TiC changed to grayish white after treatment, suggesting the formation of a TiO_2 phase. Temperatures used for annealing TiC are denoted in sample code as CTxxx (where "xxx" denotes the temperature, in °C). The duration of heating is maintained at 5 h, unless it is specified as CTxxx-YY (where "YY" denotes the time of heating, in hours).

Table 1. Experimental Conditions Used for the Preparation of Various C-TiO_2 Substrates

sample code[a]	treatment temperature (°C)	duration of heating (h)
CT250	250	5
CT300	300	5
CT350	350	5
CT350-10	350	10
CT350-15	350	15
CT350-24	350	24
CT350-30	350	30
CT350-68	350	68
CT400	400	5
CT500	500	5

[a]Temperatures used for annealing TiC are denoted in the sample code as CTxxx (where "xxx" denotes temperature in °C). The duration of heating is maintained at 5 h unless the sample code is specified as CTxxx-YY (where "YY" denotes the time of heating in hours).

Samples for Raman spectroscopic studies were prepared as follows. A known concentration of analyte (4-MBA and 4-NTP) was mixed with 2 mg of C-TiO_2 substrate via sonication for 2 h. Subsequently, 10 μL of the suspension was drop-cast onto precleaned Si wafers, followed by evaporation of solvent under ambient conditions. When oxidized TiC film was used, 10 μL of analyte were drop-coated on it, the solvent was evaporated under ambient conditions, and the film was subsequently used in dry state for Raman spectroscopic studies.

Recyclability experiments were carried out as follows. The substrate with adsorbed analyte was exposed to visible radiation (tungsten-halogen lamp) with an intensity of 0.27 W for ~5 h at 25 °C. Exposure to visible light results in the removal of adsorbed analyte, thus renewing the C-TiO_2 surface for subsequent use. The surface was washed well with distilled water and air-dried. Subsequent adsorption of analyte was carried out as mentioned earlier and Raman spectra were then recorded. This procedure of regeneration of substrate was repeated several times to probe the stability of substrate and reproducibility of Raman signals.

Materials: Characterization. The C-TiO_2 samples were characterized using UV−vis spectroscopy (UV-vis-NIR spectrophotometer, Perkin−Elmer, Model Lambda 750) in the diffused reflectance mode, powder X-ray diffraction (XRD) (Bruker, Model D8 with Cu Kα excitation), and X-ray photoelectron spectroscopy (XPS) (Thermofisher Scientific, U.K) with Al Kα excitation (1486.3 eV). An analysis of the XPS data has been carried out using XPSPEAK41/CASA freeware software. Shirley and linear algorithm were adopted for background correction. Photoluminescence (PL) measurements were carried out using Horiba−Jobin Yvon micro PL and LabRAM spectrometers equipped with an He−Cd laser (325 nm) as a source of excitation. The acquisition time used for PL measurements was 5 s. Raman spectra were recorded (LabRAM HR, Horiba Jobin Yvon, France) using a 514.5-nm, air-cooled Ar^+ laser with 50× objective and with laser intensity of 1.3 mW. Data acquisition time was kept at 20 s for all samples, until otherwise stated. Recycling of substrates was carried out by illuminating with a 250-W quartz tungsten halogen (QTH) lamp (Model 6334NS) equipped with a liquid filter (Newport Corporation, USA). The morphology of the samples was studied using a scanning electron microscopy system (SIRION/FEI, scanning electron microscopy (SEM)) equipped with an energy-dispersive X-ray analysis (EDAX) facility. Samples for SEM were prepared by drop-casting ethanolic dispersions of the powder onto precleaned Si substrates, followed by drying under vacuum for 12 h. The C-TiO_2 coatings on a SS substrate were used as such for SEM studies.

RESULTS AND DISCUSSION

Figure 1 shows the XRD patterns of thermally annealed TiC under different conditions, and the extent of oxidation clearly

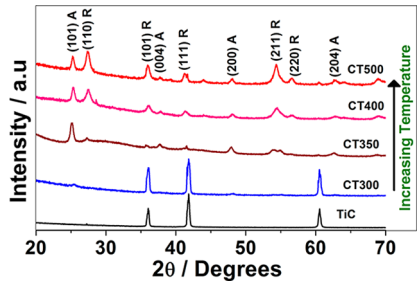

Figure 1. XRD patterns of TiC samples annealed at different temperatures for 5 h. (A and R represent anatase and rutile, respectively.) Temperatures used for annealing TiC are denoted in the sample code as CTxxx ("xxx" denotes temperature in °C). The direction of the arrow indicates the increase in the temperature of annealing.

can be controlled by varying the temperature used to anneal the material. Figure 1 shows data corresponding to conditions where TiC powder is subjected to different temperatures for a period of 5 h. It is quite evident that complete conversion of TiC to TiO_2 can be realized only after heating the specimen to a temperature of 350 °C and beyond, where reflections corresponding to TiC are completely absent. The cubic TiC (JCPDF 73-0472) phase disappears in samples heated above 350 °C (CT350, CT400, and CT500) and new reflections are identified as both anatase (JCPDF 21-1272) and rutile (JCPDF 21-1276) phases of TiO_2. The relative amounts of anatase to rutile can be varied depending on thermal treatment and is determined according to a procedure described earlier and based on the following relationship:[35]

$$W_R = \frac{1}{1 + 0.8(I_A/I_R)}$$

$$W_A = 1 - W_R$$

where W_A and W_R are the weight contents of anatase and rutile phases, respectively; I_A and I_R are intensities of diffraction peaks corresponding to anatase (101) and rutile (110), respectively. The values obtained are given in Table 2. As evident from the table, the amount of rutile phase increases as the treatment temperature increases. The anatase-to-rutile transition occurs at relatively low temperatures and is likely to be due to the presence of carbon, as reported in the literature.[36,37] Cheng et al.[36] reported a carbon-assisted phase transition of TiO_2 from anatase to rutile and suggested that carbon generates oxygen vacancies by reacting with oxygen of TiO_2, thus facilitating phase transition from anatase to rutile. As shown in Figure S1 in the Supporting Information, the rutile phase can be exclusively obtained by annealing TiC powders at 800 °C for 5 h, although exclusive anatase phases are not obtained under the experimental conditions used in the present studies. Both TiC powder and film show similar behavior.

Table 2. Relative Amounts of Anatase and Rutile Phases of Samples Prepared under Different Conditions Based on the Reported Procedure[a]

sample	anatase (wt %)	rutile (wt %)
CT350	90	10
CT400	51	49
CT500	35	65
CT800	0	100

[a]Procedure for the calculation of contents of anatase and rutile is taken from ref 35.

SEM. Morphology of TiC and C-TiO_2 powders prepared under different conditions are shown in Figure 2. The SEM pictures of commercial TiC powder indicate the presence polydisperse (5−10 μm) particles of various shapes and sizes. As shown in Figure 2, there is a certain degree of change in physical appearance after thermal treatment at different temperatures. It is also noticed that the sample is comprised of particles of sizes ranging from 0.2 μm to 6 μm (long axis of the particle). The samples heated at 350 °C for different periods of time also behave very similarly (see Figure S2 in the Supporting Information). The EDAX analyses show the presence of varied amounts of carbon for different samples prepared under different conditions (see Table ST1 in the Supporting Information)]. Though qualitative, the variation is similar to the trend observed based on XPS analysis as given below. Microstructural analysis of TiC and CT350-15 films coated on SS revealed well-defined smooth surfaces without any detectable change in morphology on heating (see Figure S3 in the Supporting Information). The XRD patterns show some broadness in the peaks (Figure 1). The crystallite size determined from the full width at half-maximum (FWHM) of the XRD peaks, using the Scherrer equation (few to several tens of nanometers, 40−50 nm), does not correspond to the size observed in the micrographs (SEM). It should be noted that the sample heated to 800 °C shows sharp peaks in XRD (see Figure S1 in the Supporting Information, rutile phase), although the size and shape do not change much, compared to a sample heated at 350 °C. Hence, it is speculated that there may be slight amorphous nature of the material that is observed in XRD (as broad peaks) for samples annealed at 350 °C.

UV−vis Spectral Analysis. Metal/nonmetal doping has a profound influence on light absorption characteristics of TiO_2.[7,37−40] Figure S4a in the Supporting Information depicts a comparison of UV−vis spectra between undoped and C-doped TiO_2 prepared at different temperatures for a period of 5 h. The data reveal two prominent features, namely, a red shift of the absorption edge upon C-doping and enhanced absorption in the visible region (400−800 nm). These observations confirm successful doping of carbon into the TiO_2 lattice. It has been well-documented that a shift in absorption edge upon doping with carbon introduces a series of localized occupied states in the band gap, and this causes a red shift in the absorption edge into the visible region.[41,42] The long tail in the visible region is attributed to the presence of carbonate species.[13,41,43] It is also worth mentioning that the extent of a red shift in the absorption edge varies with experimental conditions (see Figure S4a and S4b in the Supporting Information). This could be due to the presence of different amounts of dopant, because its quantity depends on the conditions employed during thermal treatment. Furthermore, variation in the intensity of tail that extends into the visible region as a function of time also suggests the presence of varied amounts of carbon/carbonate species. Among the investigated samples, C-TiO_2 prepared at 500 °C for 5 h (CT500) seems to have large amounts of carbon dopant, because of its high-intensity visible tail. Furthermore, C-TiO_2 prepared at 350 °C for 15 h (CT350-15) shows high absorbance in the visible range, compared to samples prepared at the same temperature for long periods of time. This could be due to the release of carbon from the TiO_2 lattice during an extended period of

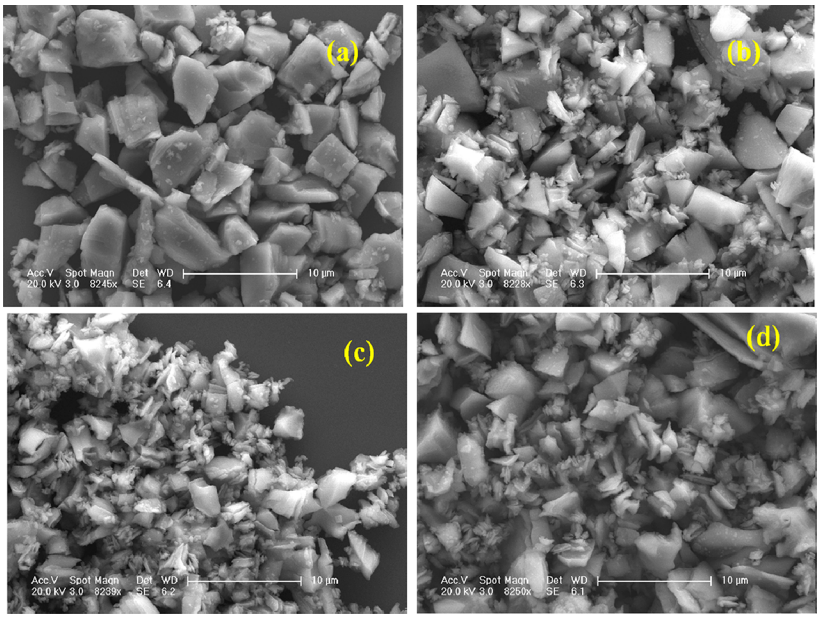

Figure 2. SEM images of (a) as-obtained commercial TiC powder, and C-TiO_2 prepared at (b) 350, (c) 400, and (d) 500 °C for 5 h.

heating.[40] Dong et al. have reported similar observations where the carbon dopant in the C-TiO_2 is released when C-TiO_2 is subjected to thermal treatment.[40] Similarly, a decrease in visible absorption for samples annealed for long periods of time may be attributed to the release of carbon from TiO_2.

The effect of adsorption of analytes on C-TiO_2 is shown in Figure 3. There is a slight blue shift of ~6−8 nm in the

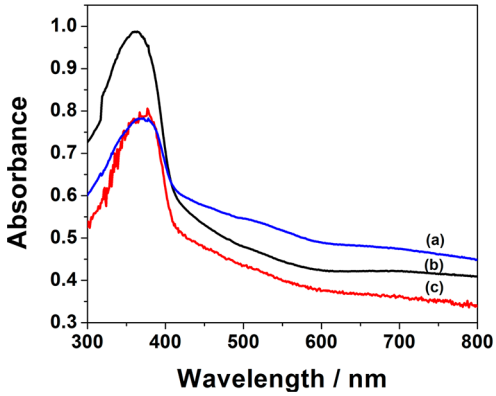

Figure 3. UV−vis spectra of (a) unmodified C-TiO_2 and C-TiO_2 modified with (b) 4-MBA and (c) 4-NTP. (C-TiO_2 substrate prepared at 350 °C for 15 h.)

absorption threshold observed for 4-MBA- and 4-NTP-modified C-TiO_2, compared to unmodified C-TiO_2. The magnitude of the shift is larger in the case of the 4-NTP-modified C-TiO_2 than that observed for the 4-MBA-modified one. Also, the extent of the blue shift is different for different samples and CT350-15 shows a large shift, compared to other samples prepared at 350 °C for different periods of time. Annealing temperature/time leads to two opposing effects: one leads to an increase in the dopant concentration (C-TiO_2) and another leads to loss of carbon from lattice.[40] Coupling between molecule and TiO_2 is expected based on the shift in absorption threshold after surface modification. Similar observations have been reported by several other groups.[10,44,45] The change observed in absorption edge depends on the analyte used.[14,17] The direction of charge transfer can be either from analyte to TiO_2, as observed in the case of ene-diol-modified TiO_2,[16,17] or from TiO_2 to analyte as reported for TiO_2 modified with sulfur-containing molecules.[14,15] 4-MBA and 4-NTP have low-lying unfilled π^* orbitals, which can readily act as electron acceptors and, hence, charge transfer is expected to be from TiO_2 to analyte.

XPS Analysis. XPS is a very powerful technique that helps in understanding the surface composition and chemical state of different constituents. Figures 4a and 4b show deconvoluted XPS spectra of the C 1s and Ti 2p regions, respectively, for CT350-15, along with its precursor, TiC. As the data indicate, the peak located at a binding energy (BE) value of 281.8 eV (Figure 4a) is characteristic of TiC (originates from Ti−C linkage),[41,46] and is absent in the case of CT350-15, indicating a conversion of TiC into C-TiO_2. Peaks observed at BE values of 284.5, 286.4, and 288.3 eV for C-TiO_2 correspond to elemental carbon, C−O-like species, and C═O, COO bonds, respectively.[47] The presence of a peak at 288.3 eV also indicates the formation of C−O bonds due to the replacement of the Ti atom by C in the lattice of TiO_2 that forms the Ti−O−C structure.[41,42] Hence, the peak observed at 288.3 eV may have contributions from both environments. Based on the above observations, it is confirmed that self-doping of carbon occurs during the thermal annealing of TiC powder. The formation of Ti−O−C from TiC by chemical treatment has been reported earlier.[41,42] XPS data support UV−vis data where the long tail in the visible region is attributed to the presence of a carbon-based species, which, in turn, is due to carbon occupying interstitial sites (C_I) of the TiO_2 lattice.[12,41] The interstitial sites result in energy states (S_I) below the conduction band and contribute partially to visible absorption in the case of C-TiO_2.[12,41] The transformation of TiC to C-TiO_2 has also been followed based on a deconvoluted Ti 2p spectral region (see Figure 4b). Peaks observed for the TiC phase include 455.1 eV (Ti $2p_{5/2}$) and 461.1 eV (Ti $2p_{3/2}$), as reported earlier,[41,42,46] while peaks at 458.8 and 464.7 eV correspond to the TiO_2 phase.[41,42,46] The disappearance of peaks corresponding to the TiC phase and the retention of peaks corresponding to the TiO_2 phase in the case of

dx.doi.org/10.1021/am300349k | ACS Appl. Mater. Interfaces 2012, 4, 3818−3828

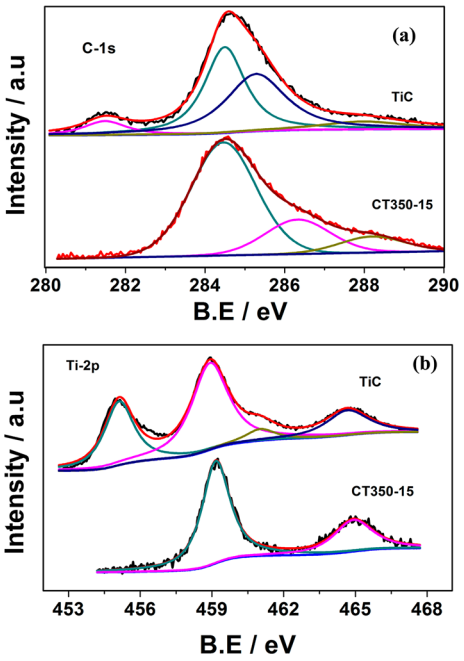

Figure 4. Deconvoluted XPS spectra of (a) C 1s and (b) Ti 2p regions for TiC and C-TiO_2 prepared at 350 °C for 15 h (CT350-15). Background correction was carried out using the Shirley algorithm.

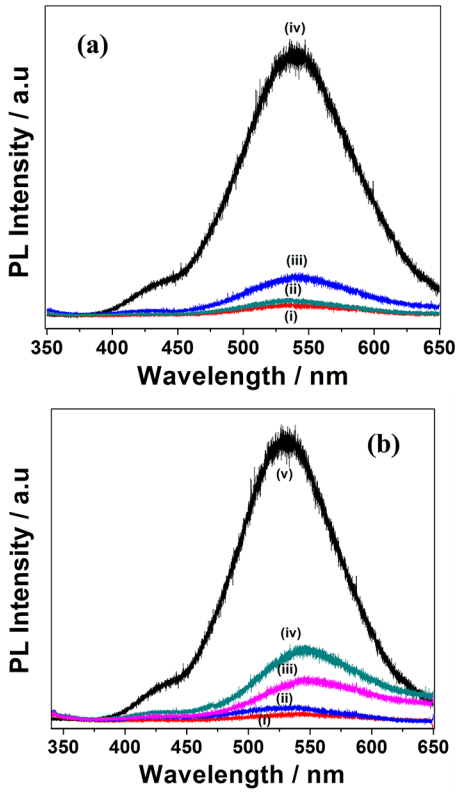

Figure 5. (a) Photoluminescence (PL) emission spectra of C-TiO_2 samples prepared at 350 (spectrum i), 400 (spectrum ii), 500 for 5 h (spectrum iii), and P25-TiO_2 (spectrum iv). (b) PL emission spectra of C-TiO_2 prepared at 350 °C for 15 h (spectrum i), 24 h (spectrum ii), 30 h (spectrum iii), and 68 h of heating (spectrum iv), and P25-TiO_2 (spectrum v). Excitation source used is 325 nm (He−Cd laser).

CT350-15 confirms the conversion of TiC to TiO_2. The existence of carbonate-like species is confirmed using XPS measurements. The O 1s region (see Figure S5 in the Supporting Information) reveals two peaks, located at BE values of 529.8 and 532 eV, which are attributed to lattice oxygen of TiO_2 and oxygen in the carbonate species, respectively.[48,49] Similar observations have been found in all the samples. Quantitative analysis has been carried out to decipher the carbon content in the sample using the C 1s (288.3 eV) region, and the details of various parameters used for calculations are given in the Supporting Information. It is found that carbon content varies in the order

$$\text{CT350 (0.21)} < \text{CT400 (0.23)} < \text{CT500 (0.24)}$$

corroborating UV−vis data. The value in brackets indicates the quantity of carbon present in the sample (in units of at. %). The carbon content obtained using elemental analysis also follows a similar pattern.

Photoluminescence Studies. Photoluminescence (PL) is a nondestructive and sensitive tool used to study the photophysical and photochemical properties of materials.[50−52] Room-temperature PL spectra are recorded in solid state by exciting the samples with 325 nm irradiation (He−Cd laser) with a spot size of ∼1 μm (Figure 5). It is quite evident that all samples show broad emission with two distinguishable peaks: one at 420 nm and another at 540 nm. The former is attributed to be due to shallow trap state emission, and it is reported to be due to bulk phenomenon.[53] The appearance of green emission at 540 nm is assigned to radiative recombination of trapped excitons at under-coordinated surface defect sites.[53] The shallow traps mainly originate from oxygen vacancy defect sites located at various energy levels.[54] It has been reported that the visible emission arises from energy levels of electrons trapped in oxygen vacancies.[54] It is understood that these levels can be in the range of 0−1 eV below the conduction band level. In the present study, the presence of oxygen vacancies seems to be responsible for the observed green emission. Furthermore, PL intensity is greatly quenched in C-doped TiO_2 samples. Figure 5a shows the effect of annealing temperature (to prepare C-TiO_2 from TiC) on PL emission spectra. As is evident from Figure 5a, the extent of quenching is larger in C-TiO_2 prepared at 350 °C for 5 h (CT350) than that observed for samples prepared at 400 and 500 °C for 5 h (CT400 and CT500, respectively). Effective inhibition of recombination of electrons and holes due to carbon doping in C-TiO_2 is likely to be based on the following pathways as reported earlier.[12,55] First, the holes are trapped by surface hydroxyl groups and form hydroxyl radicals that may suppress electron−hole recombination which will reduce the PL intensity.[55] Another reason could be the formation of oxygen vacancies upon carbon doping, as suggested by earlier theoretical and experimental investigations.[12,55] Oxygen vacancies trap electrons while doped carbon trap holes and, in turn, PL intensity decreases. Beyond a threshold temperature (350 °C), PL intensity increases as shown in Figure 5a. This may be attributed to an increased dopant quantity where excess dopant itself may act as recombination centers.[56] The duration of thermal treatment also influences the extent of quenching (Figure 5b). Samples prepared at 350 °C for 15 h (CT350-15) show diminished intensity over other samples. The PL intensity decreases in the order CT350-15 < CT 350-24 < CT 350-30 < CT 350-68 < TiO_2-P25 and is likely to be due to high amounts of dopant (as evident from UV-vis data; see Figure S4b in the Supporting Information) in the case of CT350-15, but within the threshold limit.

In summary, an appropriate amount of carbon doping improves charge carrier separation by introducing surface defects.

Raman Spectroscopy. Raman spectroscopy is a very versatile tool that provides information on the crystallinity, phase composition, and defect concentration of materials. Raman spectra of annealed samples prepared under different conditions are shown in Figure S6 in the Supporting Information. The spectra consist of bands at 147 cm^{-1} (E_g), 198 cm^{-1} (E_g), 397 cm^{-1} (B_{1g}), 517 cm^{-1} (A_{1g}), and 640 cm^{-1} (E_g), corresponding to anatase phase. Bands corresponding to rutile phase appear at ~145 cm^{-1} (B_{1g}), 240 cm^{-1} (two phonon scattering), 446 cm^{-1} (E_g), and 611 cm^{-1} (A_{1g}) for samples prepared at high temperatures. The values are similar to those reported in the literature[57,58] and also consistent with the XRD results shown earlier. The presence of carbon is also confirmed by Raman spectroscopy, and the data are shown in Figure S7 in the Supporting Information. The spectra reveal the existence of two bands: one at 1386 cm^{-1} (D) and another at 1584 cm^{-1} (G), corresponding to defect and graphitic bands of carbon, respectively. It is worth mentioning that the intensities of the D and G bands vary with experimental conditions and is found to be maximum in the case of CT500 and minimum for CT350-68, corroborating UV−vis and EDAX data. In addition, the intensity of the D band decreases as the annealing temperature increases and is attributed to the improved graphitization of carbon present in TiO_2.

It has been reported by Zhang et al.[59] that carbon can diffuse from the TiC lattice to the surface and form amorphous carbon during the thermal oxidation of TiC. The onset temperature for this process is ~350−400 °C and intensity of Raman signals has been reported to improve as a function of temperature.[59] The duration of the heating has also been reported[59] to influence the intensity of Raman signals, with decreased intensity observed at long periods of heating time. This is reported to be due to the release of carbon as carbon dioxide. The thin layer of carbon formed on the surface (as the temperature increases), which is evident from Raman studies, might vary with experimental conditions.Thermal oxidation of TiC powders proceeds in different stages and the reaction is exothermic in nature, as suggested by Shimida et al.,[60] using thermal analysis and mass spectrometry. Initially, titanium oxycarbide is formed, followed by anatase formation and simultaneous evolution of carbon dioxide, as the temperature is increased. At high temperatures rutile phase gets formed. In the present study, XPS data support the existence of carbon as dopant and Raman data support the existence of amorphous carbon layer on the surface. Nevertheless, both processes impact the charge separation phenomena leading to good enhancement in Raman signals. As the annealing temperature increases, there may be loss of carbon due to the release of carbon dioxide. The exothermic nature of the process might result in high temperatures of local spots, leading to varying shapes and sizes.

Raman Spectra of 4-MBA/4-NTP Adsorbed on Various C-TiO_2 Substrates. Raman spectra are recorded using 4-MBA/4-NTP as analytes adsorbed on various C-TiO_2 substrates. It can be concluded that CT350 is the optimum composition exhibiting higher signals than that observed on substrates prepared at other temperatures (see Figure S8 in the Supporting Information). Accordingly, CT350 is chosen for further studies. Figure 6a shows Raman spectra of 4-MBA in the presence and absence of the CT350-15 substrate. Samples were prepared by drop-casting respective dispersions on pure Si, followed by drying under ambient conditions. Figure 6

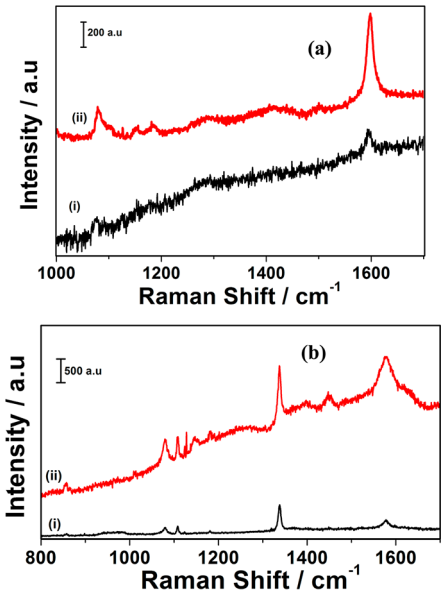

Figure 6. Raman spectra for 1 mM (a) 4-MBA and (b) 4-NTP in the absence (spectrum i) and presence (spectrum ii) of C-TiO_2 prepared at 350 °C for 15 h.

clearly shows that bands corresponding to 4-MBA get enhanced in the presence of CT350-15, which suggests good activity of C-TiO_2 toward enhancing Raman signals. Control experiments without the analyte reveal that the bands observed in the presence of analyte are solely due to adsorbed molecules and not due to the substrate (see Figure S9 in the Supporting Information). Most of the allowed vibrational bands corresponding to 4-MBA are observed and the band positions match with that of 4-MBA adsorbed on TiO_2 nanoparticles as reported earlier.[14] As shown in the Supporting Information (Table ST2), slight shifts in the band positions are observed for adsorbed analytes, compared to bulk samples. It may also be emphasized that the extent of enhancement observed is different for different modes. Two strong bands observed at 1594 cm^{-1} and 1078 cm^{-1} correspond to ν_{8a} (a_1) and ν_{12} (a_1) modes, respectively, characteristic of aromatic ring vibrations.[14,61] Apart from the two bands, there are few weak bands located at 1149 cm^{-1} and 1182 cm^{-1}; the former band is due to the ν_{15} (b_2) mode and the latter is ascribed to the ν_9 (a_1) mode of C−H deformation. Lombardi et al. have reported similar spectra for 4-MBA on TiO_2 nanoparticles.[14,15,56] Experiments carried out using CT350-15 modified with 4-NTP show enhancement, as given in Figure 6b. The spectra show intense bands at 1080, 1337, and 1578 cm^{-1} and are assigned to be due to S−C stretching vibration, $\nu_5(NO_2)$, and C═C stretching vibration of benzenyl ring, respectively.[62] Raman spectra have also been recorded on randomly selected 15 different spots on the substrate (see Figures S10a and S10b in the Supporting Information). The relative standard deviation (RSD) (ratio of standard deviation to average) corresponding to different bands for 4-MBA and 4-NTP are listed in Table 3. It is noteworthy that the RSD values are observed to be as low as 0.2, confirming uniform modification of the C-TiO_2 substrate. Zhang et al.[63] have reported similar observations with RSD values of <0.2 for Ag-coated Si nanowires using 4-aminothiophenol as the analyte. The present estimate is not based on intensity variations corresponding to a single Raman band but based on multiple bands. Raman spectrum of 4-MBA recorded by

Table 3. Peak Positions and Corresponding Relative Standard Deviation (RSD) Values for 4-MBA and 4-NTP Adsorbed onto a CT350-15 Substrate

4-MBA		4-NTP	
peak position (cm^{-1})	RSD	peak position (cm^{-1})	RSD
1078	0.18	1078	0.19
1182	0.11	1108	0.14
1594	0.15	1337	0.18
		1578	0.17

adsorbing it onto C-TiO_2 film coated on a SS substrate (prepared by heating TiC film at 350 °C for 15 h) shows similar behavior (see Figure S11 in the Supporting Information). The origin of observed enhancement in Raman signals is likely to be due to the CM type, as reported by several researchers for semiconductor substrates.[14−25] In the case of TiO_2, it has been found that the observed enhancement is due to charge-transfer interactions between TiO_2 and the analyte, 4-MBA that modify the Raman scattering cross-section of the 4-MBA, thus enhancing the signal.[14,16]

Estimation of Enhancement Factor (EF). The enhancement ability of C-TiO_2 substrates has been evaluated using the following relationship:

$$\mathrm{EF} = \left(\frac{I_R}{I_{NR}}\right)\left(\frac{N_{bulk}}{N_R}\right) \quad (1)$$

where I_R corresponds to the intensity of the analyte adsorbed on C-TiO_2 and I_{NR} is the intensity of normal Raman (NR) spectrum of the analyte without C-TiO_2. N_R and N_{bulk} respectively correspond to the number of analyte molecules adsorbed on C-TiO_2 and the number of molecules in bulk. It is evident from the above equation that accurate determination of N_R and N_{bulk} values is essential to obtain EF. The band observed at 1594 cm^{-1} in the case of 4-MBA is selected for the calculation of EF. The ratio of I_R/I_{NR} is found to be ∼10.1 for 4-MBA on the CT350-15 substrate.

N_{bulk} is estimated with the aid of the laser spot size (∼1.2 μm), the confocal depth of focus (8.2 μm), and the density of 4-MBA (1.5 g cm^{-3}). N_{bulk} has been calculated according to eq 2:[64]

$$N_{bulk} = \frac{Ah\rho}{m} \quad (2)$$

where A is the area of the laser spot, h the confocal depth of focus, ρ the density of analyte, and m the molecular weight of analyte. The value of N_{bulk} is determined to be 5.5×10^{10}.

N_R is estimated by adopting the procedure reported by Kim et al.[65] The concentration of 4-MBA adsorbed on C-TiO_2 is 1×10^{-3} M, assuming that all 4-MBA molecules are adsorbed on the C-TiO_2 substrate. Thus, the number of moles of 4-MBA contributing to the Raman signal is 1×10^{-8} mol (a volume of 10 μL is used in the present studies). The area occupied by 4-MBA molecules that gives rise to the observed Raman signal may be determined using the laser spot size. Hence, the number of molecules of 4-MBA present under laser illumination can be estimated by taking the sampling area and the number of moles into account as $(1 \times 10^{-8})/\{[\pi(5\ \mathrm{mm})^2] \times [\pi(0.6\ \mu\mathrm{m})^2]\}$, i.e., $N_R = 8.85 \times 10^7$. This leads to EF of the order of $(6.2 \pm 0.8) \times 10^3$. Similar treatment is adopted for 4-NTP adsorbed on C-TiO_2, and the EF is determined to be $(7.7 \pm 1.2) \times 10^3$ (corresponding to a band located at 1578 cm^{-1}) and $(1.7 \pm 1.2) \times 10^3$ (corresponding to a band located at 1337 cm^{-1}). The values obtained in the present study are quite comparable with values of ∼10^3 observed on ZnS [21], 10^2 observed on CdS,[20] and 10^3 observed on ZnO,[66] wherein chemical enhancement is reported to be responsible for the observed effect.

Concentration-dependent studies have been carried out using the CT350-15 substrate with 4-NTP and 4-MBA analytes. The detection limit is found to be several micromolar (see Figure S12 in the Supporting Information), as observed on other substrates based on the charge-transfer mechanism.[15,21,66] Control experiments on 4-MBA adsorbed on an untreated TiC substrate does not show any enhancement (see Figure S8 in the Supporting Information). The presence of trace amounts of TiC in C-TiO_2 substrates decreases the intensity of the Raman signals. Thus, the observed enhancement effect is only due to C-TiO_2 and not its precursor, TiC. Studies carried out as a function of the excitation wavelength reveal that the most-intense Raman signals are observed with 514.5 nm as the excitation source over 633 and 785 nm (see Figure S13 in the Supporting Information). This is due to the fact that the charge-transfer complex formed between C-TiO_2 and 4-MBA/4-NTP absorbs at wavelengths of ∼500−520 nm.

The effect of carbon doping on the enhancement of the Raman signals for 4-MBA is followed by carrying out control experiments with P25-TiO_2 as the substrate. As shown in Figure 7, signals corresponding to 4-MBA/4-NTP are

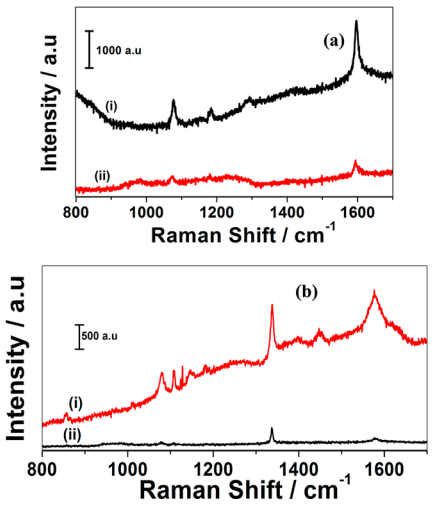

Figure 7. Raman spectra of (a) 1 mM 4-MBA and (b) 1 mM 4-NTP adsorbed on C-TiO_2 prepared at 350 °C for 15 h (spectrum i) and P-25 TiO_2 powder (spectrum ii).

significantly enhanced when the analyte is adsorbed on CT350-15, compared to that observed on pure TiO_2 under identical conditions. To understand the effect of dopant concentration, various C-TiO_2 substrates (prepared by annealing TiC at 350 °C for different periods of time) have been used to study the Raman spectra of 4-MBA (Figure 8a). There seems to be a strong correlation between PL and Raman data wherein the CT350-15 substrate possesses a lower PL intensity with higher enhancement in Raman signals for the analyte molecule (4-MBA) (see Figure 8b), compared to other substrates. Based on the above observations, it can be envisaged that surface defects play a significant role in the observed enhancement. Xue et al.[67] have reported similar enhancement on Co-doped ZnO, and the enhancement is

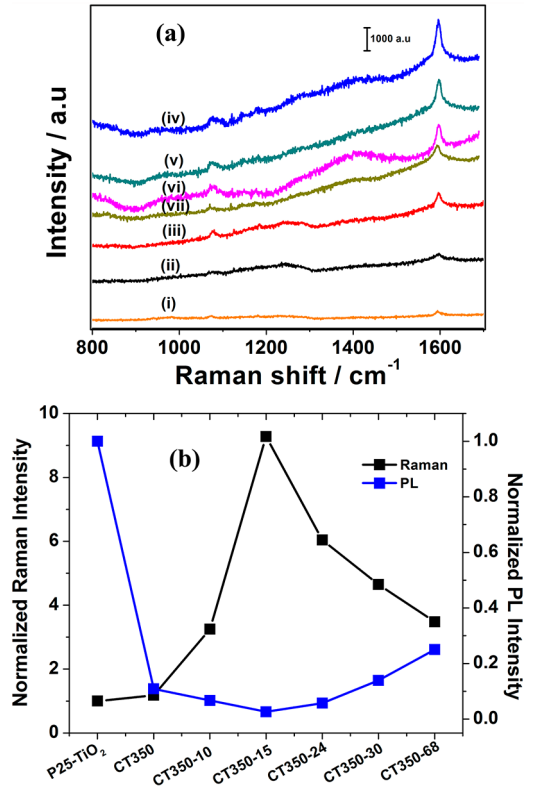

Figure 8. (a) Raman spectra of 0.5 mM 4-MBA adsorbed on P25-TiO_2 (spectrum i) and on various C-TiO_2 prepared at 350 °C for periods of 5 h (spectrum ii), 10 h (spectrum iii), 15 h (spectrum iv), 24 h (spectrum v), 30 h (spectrum vi), and 68 h (spectrum vii). (b) Normalized Raman (NR) intensity (black) for the band at 1594 cm^{-1} is given along with normalized PL intensity (blue) for various CT350 substrates.

attributed to surface defects upon Co doping. Yang et al.[56] show the effect of Zn doping in TiO_2, where it is claimed that the presence of surface defects leads to the observed enhancement. The surface defects induced by carbon doping play a similar role for efficient charge transfer observed in the present studies. It is worth mentioning that nonmetal-doped TiO_2 substrates are expected to be superior photocatalyts over transition-metal-doped TiO_2, because of the poor photostability of the latter.[12]

Increased charge transfer transitions between TiO_2 and analyte may be responsible for the enhancement of Raman signals. Carbon doping of TiO_2 decreases the rate of recombination of photogenerated carriers (electrons and holes) and allows electrons to jump into lowest unoccupied molecular orbital (LUMO) of the analyte. Thus, in accordance with PL and Raman data, the dopant introduces surface defects (possibly, oxygen vacancies) that lead to the presence of certain trap states within the band gap. The surface states trap electrons, inhibiting charge carrier recombination thereby enhancing charge transfer and improved Raman activity. Hence, it is suggested that carbon dopant plays a dual role. First, it improves the lifetime of charge carriers by creating surface levels, and second, it helps to shuttle electrons from TiO_2 to the LUMO of analyte molecule via trap states.

Since the observed enhancement is due to charge-transfer interactions between molecules and substrate, substituent groups on the analyte molecule will influence the extent of enhancement of Raman signals. As shown by Figure S14 in the Supporting Information, the Raman intensity for 4-NTP adsorbed on the CT350-15 substrate is relatively higher than that of 4-MBA, because of the effective electron-withdrawing nature of the $-NO_2$ group over the $-COOH$ group. Similar observations have been reported on TiO_2[14] and ZnO[67] nanoparticles as substrates.

The C-TiO_2 substrates can be regenerated with the assistance of light. The CT350-15 sample after adsorption and analysis of 4-MBA is illuminated using a tungsten halogen lamp with an intensity of 0.27 W for 5 h. Figure 9a presents data where the

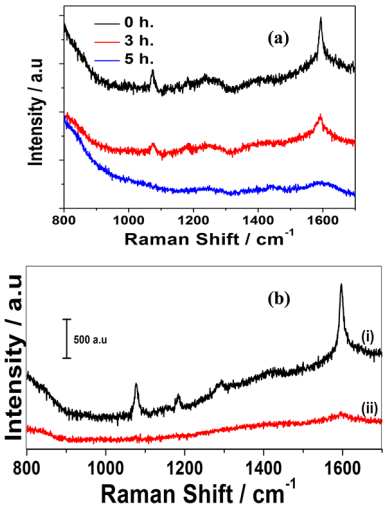

Figure 9. Raman spectra of 1 mM 4-MBA showing (a) the effect of illumination time (no filter). (b) Raman spectra of 1 mM 4-MBA before illumination (spectrum i) and after the illumination for 5 h (spectrum ii), in the presence of a green filter. Substrate used is C-TiO_2 prepared at 350 °C for 15 h.

Raman spectral intensity decreases as the time of illumination increases and, finally, the signal fades off completely. After 5 h of continuous illumination, no band corresponding to 4-MBA could be detected, suggesting regeneration of the substrate under visible-light conditions. It is confirmed by recording Raman spectra on 15 different spots over the entire area of the sample under investigation (see Figure S15 in the Supporting Information). Experiments have also been performed using a green filter that cuts off light below a wavelength of 450 nm and the data are shown in Figure 9b. As indicated in Figure 9b, the substrates can be regenerated using visible light after illuminating for 5 h.

To check the robustness of regeneration, the sequence shown in Scheme 1 is followed and Raman spectra recorded. First, the CT350-15-coated Si surface is modified by drop-coating 10 μL of 1 mM 4-MBA and dried. Raman spectra are recorded before and after illumination for 5 h (see Figure 10). The origin of regeneration of substrates is due to the self-cleaning action of TiO_2. Highly reactive hydroxyl ($OH^{\bullet}$) radicals are formed upon illumination that degrade organic molecules adsorbed on the surface. Recently, Liu et al.[30] and Alessandri et al.[33] proposed similar strategies to regenerate Raman substrates using UV light. The use of visible radiation, as opposed to UV radiation, opens up the possibility of regeneration using sunlight.

dx.doi.org/10.1021/am300349k | ACS Appl. Mater. Interfaces 2012, 4, 3818−3828

Scheme 1. Schematics of Regeneration Protocol Used

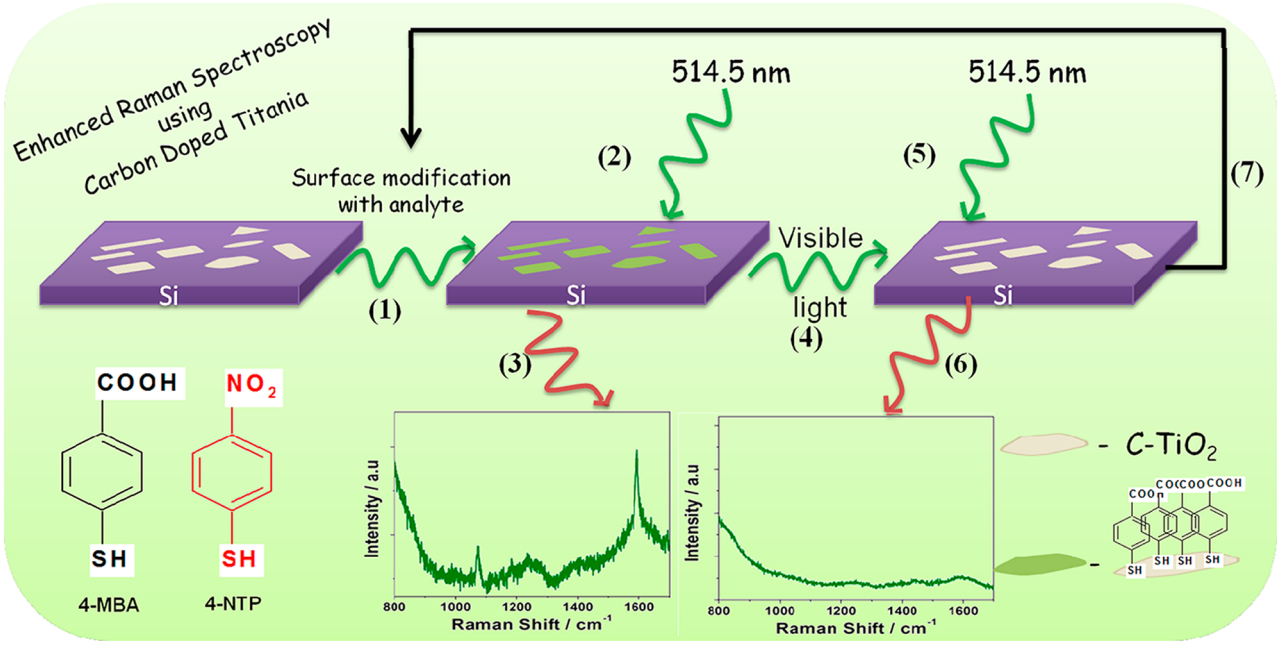

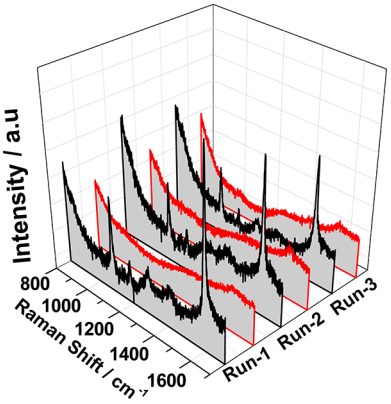

Figure 10. Raman spectra of 1 mM 4-MBA on CT350-15 (black) and corresponding regenerated surface (red) after visible-light illumination. Three runs are given.

CONCLUSIONS

We have explored the use of C-TiO_2 as an effective substrate for enhancing Raman signals of molecules adsorbed on it. The presence of carbon in the TiO_2 lattice induces facile charge transfer between the molecule and substrate by creating surface defects, and, hence, an enhanced Raman signal is observed. It is also shown that, beyond a certain threshold, carbon doping actually reduces the enhancement, because surface defects themselves act as recombination centers, thus reducing charge separation. The present substrates can be regenerated with the help of the self-cleaning action of TiO_2 by shining visible light for a particular period of time.

ASSOCIATED CONTENT

Supporting Information

patterns patterns of C-TiO_2 prepared at 350 and 800 °C for 5 h (Figure S1), SEM images of various C-TiO_2 substrates prepared at 350 °C for different periods of time (Figure S2), SEM images TiC film and C-TiO_2 film prepared at 350 °C for 15 h (Figure S3), UV−vis spectra of C-TiO_2 prepared under different experimental conditions (Figure S4), deconvoluted O 1s XPS spectra of C-TiO_2 prepared at 350 °C for 5 h (Figure S5), Raman spectra of various C-TiO_2 substrates prepared at different temperatures for a period of 5 h (Figure S6), Raman spectra in the region of 1100−1700 cm^{-1} of various C-TiO_2 substrates prepared at different temperatures for a period of 5 h (Figure S7), Raman spectra of 0.5 mM 4-MBA adsorbed on various C-TiO_2 substrates prepared at different temperatures for a period of 5 h (Figure S8), Raman spectra of various C-TiO_2 substrates prepared at different temperatures for a period of 5 h, in the absence of analyte (Figure S9), Raman spectra of 4-MBA and 4-NTP adsorbed on C-TiO_2 prepared at 350 °C for 15 h, recorded over 15 randomly selected spots on the substrate (Figure S10), Raman spectra of 1 mM 4-MBA adsorbed on C-TiO_2 film prepared at 350 °C for 15 h from TiC film (Figure S11), concentration-dependent Raman spectra corresponding to 4-MBA, 4-NTP adsorbed on C-TiO_2 prepared at 350 °C for 15 h (Figure S12), effect of excitation wavelength on Raman spectrum of 1 mM 4-MBA adsorbed on CT350-15 (Figure S13), Raman spectra of 1 mM 4-MBA and 1 mM 4-NTP adsorbed on C-TiO_2 prepared at 350 °C for 15 h (Figure S14), Raman spectra of C-TiO_2 modified with 1 mM 4-MBA before and after illumination, on 15 randomly selected regions (Figure S15), and chemical structures of 4-MBA and 4-NTP (Figure S16). Carbon content and C/Ti ratio obtained from EDAX analysis (Table ST1), and Raman bands and band assignments corresponding to 4-MBA and 4-NTP in the presence and absence of a C-TiO_2 substrate (Table ST2). This material is available free of charge via the Internet at http://pubs.acs.org.

AUTHOR INFORMATION

Corresponding Author

*Tel.: +91 80 22933315. Fax: +91 80 23600085. E-mail address: sampath@ipc.iisc.ernet.in.

Notes

The authors declare no competing financial interest.

■ ACKNOWLEDGMENTS

We thank the Centre for Nanoscience and Engineering (CeNSE), IISc for PL measurements. V.K. thanks the Council of Scientific and Industrial Research (CSIR), India for financial assistance. We acknowledge the Department of Science and Technology (DST), New Delhi, India for financial support.

■ REFERENCES

(1) Paunesku, T.; Rajh, T.; Wiederrecht, G.; Maser, J.; Vogt, S.; Stojicevic, N.; Protic, M.; Lai, B.; Oryhon, J.; Thurnauer, M.; Woloschak, G. *Nat. Mater.* **2003**, *2*, 343−346.
(2) Rajh, T. *Nat. Mater.* **2006**, *5*, 347−348.
(3) Clarke, S. J.; Hollmann, C. A.; Zhang, Z.; Suffern, D.; Bradforth, S. E.; Dimitrijevic, N. M.; Minarik, W. G.; Nadeau, J. L. *Nat. Mater.* **2006**, *5*, 409−417.
(4) Tepavcevic, S.; Darling, S. B; Dimitrijevic, N. M.; Rajh, T.; Sibener, S. J. *Small* **2009**, *5*, 1776−1783.
(5) Hu, X.; Li, G.; Yu, J. C. *Langmuir* **2010**, *26*, 3031−3039.
(6) Cropek, D.; Kemme, P. A.; Makarova, O. V.; Chen, L. X.; Rajh, T. *J. Phys. Chem. C* **2008**, *112*, 8311−8318.
(7) Dong, F.; Wang, H.; Wu, Z. *J. Phys. Chem. C* **2009**, *113*, 16717−16723.
(8) Chen, X.; Liu, L.; Yu, P. Y.; Mao, S. S. *Science* **2011**, *331*, 746−750.
(9) Fujishima, A.; Honda, K. *Nature* **1972**, *238*, 37−38.
(10) Rajh, T.; Chen, L. X.; Lukas, K.; Thurnauer, M. C.; Tiede, D. M. *J. Phys. Chem. B* **2002**, *106*, 10543−10552.
(11) Rajh, T.; Nedeljkovic, J. M.; Chen, L. X.; Poluektov, O.; Thurnauer, M. C. *J. Phys. Chem. B* **1999**, *103*, 3515−3519.
(12) Valentin, C. D.; Pacchioni, G.; Selloni, A. *Chem. Mater.* **2005**, *17*, 6656−6665.
(13) Sakthivel, S.; Kisch, H. *Angew. Chem., Int. Ed.* **2003**, *42*, 4908−4911.
(14) Yang, L.; Jiang, X.; Ruan, W.; Zhao, B.; Xu, W.; Lombardi, J. R. *J. Phys. Chem. C* **2008**, *112*, 20095−20098.
(15) Yang, L.; Jiang, X.; Ruan, W.; Zhao, B.; Xu, W.; Lombardi, J. R. *J. Raman Spectrosc.* **2009**, *40*, 2004−2008.
(16) Musumeci, A.; Gosztola, D.; Schiller, T.; Dimitrijevic, N. M.; Mujica, V.; Martin, D.; Rajh, T. *J. Am. Chem. Soc.* **2009**, *131*, 6040−6041.
(17) Hurst, S. J.; Fry, H. C.; Gosztola, D. J.; Rajh, T. *J. Phys. Chem. C* **2011**, *115*, 620−630.
(18) Wang, Y.; Hu, H.; Jing, S.; Wang, Y.; Sun, Z.; Zhao, B.; Zhao, C.; Lombardi, J. R. *Anal. Sci.* **2007**, *23*, 787−791.
(19) Sun, Z.; Zhao, B.; Lombardi, J. R. *Appl. Phys. Lett.* **2007**, *91*, 221106−1−3.
(20) Wang, Y.; Sun, Z.; Wang, Y.; Hu, H.; Zhao, B.; Xu, W.; Lombardi, J. R. *Spectrochim. Acta A* **2007**, *66*, 1199−1203.
(21) Wang, Y.; Sun, Z.; Hu, H.; Jing, S.; Zhao, B.; Xu, W.; Zhao, C.; Lombardi, J. R. *J. Raman Spectrosc.* **2007**, *38*, 34−38.
(22) Hayashi, S.; Koh, R.; Ichiyama, Y.; Yamamoto, K. *Phys. Rev. Lett.* **1988**, *60*, 1085−1088.
(23) Fu, X.; Pan, Y.; Wang, X.; Lombardi, J. R. *J. Chem. Phys.* **2011**, *134*, 024707-1−024707-5.
(24) Wang, Y.; Zhang, J.; Jia, H.; Li, M.; Zeng, J.; Yang, B.; Zhao, B.; Xu, W.; Lombardi, J. R. *J. Phys. Chem. C* **2007**, *112*, 996−1000.
(25) Quagliano, L. G. *J. Am. Chem. Soc.* **2004**, *126*, 7393−7398.
(26) King, F. W.; Van Duyne, R. P.; Schatz, G. C. *J. Chem. Phys.* **1978**, *69*, 4472−4481.
(27) Haynes, C. L.; McFarland, A. D.; Van Duyne, R. P. *Anal. Chem.* **2005**, *77*, 338A−346A.
(28) Jiang, J.; Bosnick, K.; Maillard, M.; Brus, L. *J. Phys. Chem. B* **2003**, *107*, 9964−9972.
(29) Ma, S.; Livingstone, R.; Zhao, B.; Lombardi, J. R. *J. Phys. Chem. Lett.* **2011**, *2*, 671−674.
(30) Li, X.; Chen, G.; Yang, L.; Jin, Z.; Liu, J. *Adv. Funct. Mater.* **2010**, *20*, 2815−2824.
(31) Li, X.; Hu, H.; Li, D.; Shen, Z.; Xiong, Q.; Li, S.; Fan, H. J. *ACS Appl. Mater. Interfaces* **2012**, *4*, 2180−2185.
(32) Chen, Y.; Tian, G.; Pan, K.; Tian, C.; Zhou, J.; Zhou, W.; Ren, Z.; Fu, H. *Dalton Trans.* **2012**, *41*, 1020.
(33) Sinha, G.; Depero, L. E.; Alessandri, I. *ACS Appl. Mater. Interfaces* **2011**, *3*, 2557−2563.
(34) Lin, Y.; Bunker, C. E.; Fernando, K. A. S.; Connell, J. W. *ACS Appl. Mater. Interfaces* **2012**, *4*, 1110−1117.
(35) Liu, G.; Wang, X.; Chen, Z.; Cheng, H. M.; Lu, G. Q. *J. Colloid Interface Sci.* **2009**, *329*, 331−338.
(36) Chatterjee, A.; Wu, S.-B.; Chou, P.-W.; Wong, M. S.; Cheng, C.-L. *J. Raman Spectrosc.* **2011**, *42*, 1075−1080.
(37) Shen, M.; Wu, Z.; Huang, H.; Du, Y.; Zou, Z.; Yang, P. *Mater. Lett.* **2006**, *60*, 693−697.
(38) Wang, E.; He, T.; Zhao, L.; Chen, Y.; Cao, Y. *J. Mater. Chem.* **2011**, *21*, 144−150.
(39) Cong, Y.; Zhang, J.; Chen, F.; Anpo, M. *J. Phys. Chem. C* **2007**, *111*, 6976−6982.
(40) Dong, F.; Guo, S.; Wang, H.; Li, X.; Wu, Z. *J. Phys. Chem. C* **2011**, *115*, 13285−13292.
(41) Gu, D. E.; Lu, Y.; Yang, B. C.; Hu, Y. D. *Chem. Commun.* **2008**, 2453−2455.
(42) Yu, J.; Dai, G.; Xiang, Q.; Jaroniec, M. *J. Mater. Chem.* **2011**, *21*, 1049−1057.
(43) Wu, Z.; Dong, F.; Zhao, W.; Wang, H.; Liu, Y.; Guan, B. *Nanotechnology* **2009**, *20*, 235701−1−9.
(44) Pérez León, C.; Kador, L.; Peng, B.; Thelakkat, M. *J. Phys. Chem. B* **2006**, *110*, 8723−8730.
(45) Zhang, D.; Downing, J. A.; Knorr, F. J.; McHale, J. L. *J. Phys. Chem. B* **2006**, *110*, 21890−21898.
(46) Kiran, V.; Kalidindi, S. B.; Jagirdar, B. R.; Sampath, S. *Electrochim. Acta* **2011**, *56*, 10493−10499.
(47) Cong, Y.; Li, X.; Qin, Y.; Dong, Z.; Yuan, G.; Cui, Z.; Lai, X. *Appl. Catal., B* **2011**, *107*, 128−134.
(48) Liu, H.; Imanishi, A.; Nakato, Y. *J. Phys. Chem. C* **2007**, *111*, 8603−8610.
(49) Park, Y.; Kim, W.; Park, H.; Tachikawa, T.; Majima, T.; Choi, W. *Appl. Catal., B* **2009**, *91*, 355−361.
(50) Wang, Y. X.; Li, X. Y.; Lu, G.; Quan, X.; Chen, G. H. *J. Phys. Chem. C* **2008**, *112*, 7332−7336.
(51) Jing, L. Q.; Qu, Y. C.; Wang, B. Q.; Li, S. D.; Jiang, B. J.; Yang, L. B.; Fu, W.; Fu, H. G.; Sun, J. Z *Sol. Energy Mater. Sol. Cells* **2006**, *90*, 1773−1787.
(52) Li, F. B.; Li, X. Z. *Appl. Catal., A* **2002**, *228*, 15−27.
(53) Knorr, F. J.; Zhang, D.; McHale, J. L. *Langmuir* **2007**, *23*, 8686−8690.
(54) Serpone, N.; Lawless, D.; Khairutdinov, R. *J. Phys. Chem.* **1995**, *99*, 16646−16654.
(55) Huang, Y.; Ho, W. K.; Lee, S. C.; Zhang, L. Z.; Li, G. S.; Yu, J. C. *Langmuir* **2008**, *24*, 3510−3516.
(56) Yang, L.; Zhang, Y.; Ruan, W.; Zhao, B.; Xu, W.; Lombardi, J. R. *J. Raman Spectrosc.* **2010**, *41*, 721−726.
(57) Li, Z.; Mi, L.; Wang, P.-N.; Chen, J.-Y. *Nanoscale Res. Lett.* **2011**, *6*, 356−362.
(58) Zhang, J.; Li, M.; Feng, Z.; Chen, J.; Li, C. *J. Phys. Chem. B* **2006**, *110*, 927−935.
(59) Zhang, L.; Koka, R. V. *Mater. Chem. Phys.* **1998**, *57*, 23−32.
(60) Shimada, S. *J. Mater. Sci.* **1996**, *31*, 673−677.
(61) Michota, A.; Bukowska, J. *J. Raman Spectrosc.* **2003**, *34*, 21−25.
(62) Dong, B.; Fang, Y.; Xia, L.; Xu, H.; Sun, M. *J. Raman Spectrosc.* **2011**, *42*, 1205−1206.
(63) Zhang, B.; Wang, H.; Lu, L.; Ai, K.; Zhang, G.; Cheng, X. *Adv. Funct. Mater.* **2008**, *18*, 2348−2355.
(64) Zhu, Z.; Zhu, T.; Liu, Z. *Nanotechnology* **2004**, *15*, 357−364.

(65) Park, H. K.; Yoon, J. K.; Kim, K. *Langmuir* **2006**, *22*, 1626−1629.
(66) Wang, Y.; Ruan, W.; Zhang, J.; Yang, B.; Xu, W.; Zhao, B.; Lombardi, J. R. *J. Raman Spectrosc.* **2009**, *40*, 1072−1077.
(67) Xue, X.; Ruan, W.; Yang, L.; Ji, W.; Xie, Y.; Chen, L.; Song, W.; Zhao, B.; Lombardi, J. R. *J. Raman Spectrosc.* **2012**, *43*, 61−64.